# International Conference on Space Optics—ICSO 2014

La Caleta, Tenerife, Canary Islands

7–10 October 2014

*Edited by Zoran Sodnik, Bruno Cugny, and Nikos Karafolas*


## *Compressive sensing for hyperspectral earth observation from space*

*A. Barducci*

*D. Guzzi*

*C. Lastri*

*V. Nardino*

*et al.*

International Conference on Space Optics — ICSO 2014, edited by Zoran Sodnik, Nikos Karafolas, Bruno Cugny, Proc. of SPIE Vol. 10563, 1056353 · © 2014 ESA and CNES
CCC code: 0277-786X/17/$18 · doi: 10.1117/12.2304078

# COMPRESSIVE SENSING FOR HYPERSPECTRAL EARTH OBSERVATION FROM SPACE

A. Barducci[1], D. Guzzi[2], C. Lastri[2], V. Nardino[2], I. Pippi[2], V. Raimondi[2]

[1] *Sofasi srl Viale Alessandro Guidoni, 139 - 50127 Firenze, Italy* a.barducci@alice.it

[2] *Consiglio Nazionale delle Ricerche – Istituto di Fisica Applicata "Nello Carrara" (CNR-IFAC), Via Madonna del Piano, 10 - 50019 Sesto Fiorentino, Italy* i.pippi@ifac.cnr.it

## I. INTRODUCTION

Topical studies [1-5] demonstrate that signal acquisition can be performed at sampling frequencies far below the minimal frequency dictated by the ideal sampling theorem, a concept called "compressive sampling" (CS). This technique can be applied to signals that don't convey the entire information amount predicted by the traditional sampling theory, regardless of the maximum frequency contained in their spectrum. Signals with this intriguing characteristic are called sparse.

A basic example of sparsity is constituted by a signal having a strong average autocorrelation, like an image with large areas of constant value. The signal can still contain high spatial frequency components associated to regions of little extension showing edges or rapid variations, however the signal itself is heavily redundant. On one hand, the maximum frequency in the signal spectrum bounds the maximum information flow the signal can bring (the data rate). On the other hand, the example above shows that not all the signals having a given maximum frequency transmit the corresponding maximum flow of information. A specific (almost pathological) example of sparsity is constituted by bandpass signals whose spectrum is vanishing in a region of lower frequencies. For these signals a particular technique of undersampling has been developed in the past [6] that is able to reconstruct the signal stemming from a sampling frequency far below the Nyquist limit, therefore utilizing a lesser number of samples.

Presumably, most natural signals feature a sparsity that can not be recognized so easily. Nonetheless, some mathematical representation of a sparse signal must exist in which the number of non-trivial elements is less than that originated by a non-sparse signal. Usually, such representation is an Integral Transformation (IT) of the signal itself. The sparse mathematical representation admitted by the signal can be made accessible to a sensor, provided that a dedicated subsystem performs the involved IT before its focal plane. When radiometric and spectroscopic signals are considered, an optical subsystem would be the natural choice for optically computing this transformation.

Compressive Sampling always includes a multiplexing scheme [1,4-7] which exactly implements the mathematical transformation discussed above. It is worth noting that multiplex spectroscopy has anticipated the CS of over half a century. Multiplex spectroscopy (aka coded aperture spectroscopy) dates back to the 1949, to the pioneering works of Fellgett [8], and Goley [9] aimed to assess an experimental technique able to boost the Signal-to-Noise Ratio (SNR) of spectroscopic measurements. Then, following the diffusion of multiplex spectroscopy, i.e. Fourier Transform Spectroscopy (FTS), experimenters attempted to gain corresponding SNR benefits in the domain of panchromatic or multiband imaging, just applying a multiplex configuration to traditional instruments [10]. However, recent investigations [11-13] have shown that any multiplex techniques give rise to poorer radiometric performance with respect to the direct signal measurement operated by long-established optical configurations.

Compressive Sampling can bring many latent advantages to hyperspectral satellite imaging, since high spectral and spatial resolution can be attained with fewer detectors, lesser memory capacity, and narrower down-link bandwidth. The main advantage of CS is that compression takes place before the signal sampling, hence avoiding the acquisition of large volumes of data followed by standard signal compression. The possible impact of CS could be remarkable, motivating new investigations and research programs regarding this emerging technology. The principal disadvantage of CS is instead the intensive off-line data processing that leads to the desired source estimation.

In this paper we first summarize the CS architecture and its possible implementations for Earth observation, then we show the laboratory prototype realized in the framework of the ESA ITI-B Project titled "Hyperspectral Passive Satellite Imaging via Compressive Sensing". The prototype requires optical light modulators and 2dim detector arrays of high frame rate. The experimental test-bed adopts a push-broom imaging spectrometer with a maximum spectral resolution around 0.02 nm (FWHM) for generating a 2dim (space-spectrum) domain in the VIS-NIR spectral range. A beam-splitter at the output port of the spectrometer divides the light into two focal planes, one of which adopts the standard sampling while the other performs the CS. In this way it is possible to make a direct comparison between the CS reconstructed dataset and its expectation. The image on the CS arm is first modulated by a liquid crystal plate, then undersampled via a CCD camera that collects elements of the

requested IT. The acquisition is iterated while changing the pattern of the spatial modulator, thus measuring several elements of the involved integral transform. Information regarding the signal estimation algorithms developed in the framework of the Project have been discussed in [14].

Some preliminary measurements for the experimental assessment of CS performance and the related reconstruction errors are also shown.

## II. THE COMPRESSIVE SAMPLING ARCHITECTURE FOR EARTH OBSERVATION

Our research is being carried out in the framework of a Project titled "Hyperspectral Passive Satellite Imaging via Compressive Sensing (HPSI-CS)". The Project is being supported by the European Space Agency (ESA) by means of the ITI protocol at level B. The principal goal of the project is to explore the technological and scientific implications of compressive sensing for the remote sensing of the Earth. This activity required the collaboration of five teams with experience covering the following domains: sensor development, design of Lithium Niobate monolithic arrays, high resolution remote sensing, and signal processing. Table 1 summarizes the Institutions contributing to the HPSI-CS Project.

Table 1. Institutions contributing to the HPSI-CS Project.

| Institution | Project role |
|---|---|
| IFAC-CNR | Development of laboratory prototype (Main contractor) |
| Politecnico di Torino | Development and test of estimation algorithm (Sub contractor) |
| Università di Siena | Development and test of estimation algorithm (Sub contractor) |
| Selex ES SpA | Auditing, specs, and so forth (Sub contractor) |
| Consorzio MISTER | Development of *Monolithic Lithium Niobate* SLMs (Partner) |

Compressive sampling can be applied to passive, hyperspectral imagers operating at high spectral and spatial resolution. In this case the acquired datasets have three dimensions, two of which are spatial dimensions and the third is spectral, resulting in a very large volume of collected data. The first problem to be faced is which 2-dim domain should be compressively sampled, the remaining dimension would instead be scanned sequentially over time. Possible choices are limited to sampling compressively a $x-y$ or a $x-\lambda$ domain. Previous work [15] showed that the source information (noise free) captured by the hyperspectral instruments AVIRIS, only holds from 3 up to 6 bits per spectral sample depending on the wavelength of interest. This result confirms that reflectance spectra of natural materials observed at medium to low spectral resolution (around 10 nm of bandwidth) exhibits a significant autocorrelation, which can be relevant to the selected scheme of compressive sampling. Due to the above behavior we suppose that the $x-\lambda$ domain should be sparser than the $x-y$ one, thus we chosen the standard configuration of push-broom (dispersive) imaging spectrometer. Possible advantages expected from this configuration are listed below.

1. Mitigated ADC sampling rates, a circumstance that can result into:
    a. higher data accuracy (lower ADC noise level), and
    b. less electrical power needed for data acquisition at a given quantization accuracy.
2. Lesser memory to be installed onboard.
3. Narrower bandwidth required for the downlink.

Cost, mass, and volume budgets might be optimized adopting the compressive sampling architecture for a standard spaceborne hyperspectral sensor.

### *A. Development of the CS Prototype*

The prototype for investigating the CS technology is being developed at IFAC premises. The main instrument selected for this research is a push-broom imaging spectrometer manufactured by the Horiba Jobin Yvon firm (model iHR550) that reaches a maximum spectral resolution around 0.02 nm (FWHM) when equipped with a 2400 gr / mm grating. This instrument images a 2d spatial-spectral domain at its exit port, i.e. $x-\lambda$. The spectrometer has two input and two output ports that can be equipped with additional devices and detectors. The electro-optical elements necessary to perform the CS acquisition of the signal are hosted by the secondary port of the output focal plane. Fig. 1 depicts the optical layout placed on the secondary output focal plane of this instrument in order to perform the CS signal.

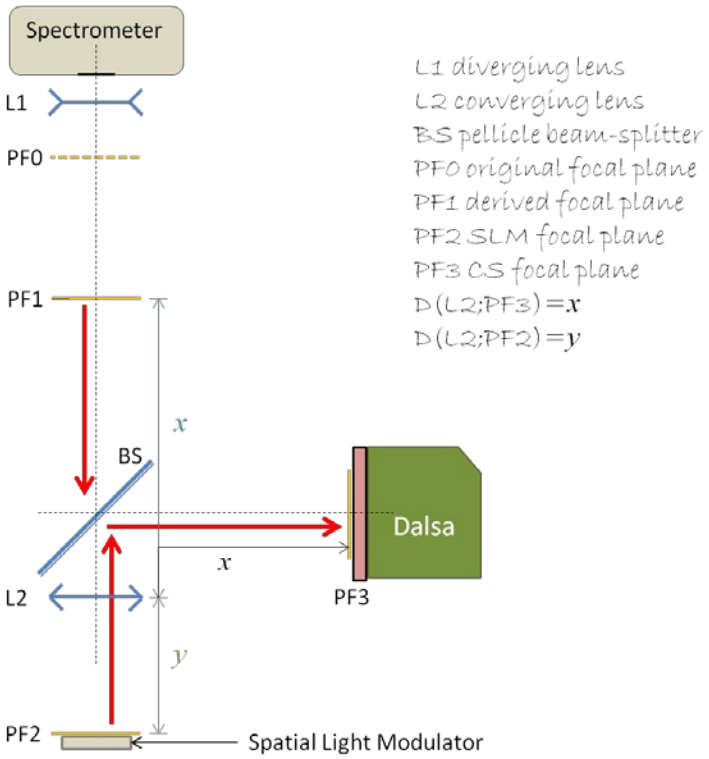


**Fig. 1.** Optical layout of CS optical assembly being installed on the secondary exit port of the instrument.

The selected Spatial Light Modulator (SLM) is a liquid crystal panel whose characteristics are reported in Table 2.

Table 2. Main characteristics of the Spatial Light Modulator (SLM) Holoeye LC-R 1080

| | |
|---|---|
| Display | LCoS Microdisplay (Reflective) |
| Resolution | 1920 x 1200 Pixel |
| Frame rate | 60 Hz |
| Pixel Pitch | 8.1 µm |

The output focal plane of the prototype holds a CCD image sensor (manufactured by Dalsa) whose main specifications are reported in Table 3.

Table 3. Main characteristics of the image sensor (Dalsa CCD)

| | |
|---|---|
| Detector | TH7888A CCD frame-transfer |
| Number of pixel | 1024 x 1024 |
| Pixel size | 14.0 µm x 14.0 µm |
| Binning | 1, 2 |
| Detector spectral range | 430 nm-1000 nm (Full Width @ QE>3%) |
| Maximum frame/rate | 60 fps |

It is worth noting that the spatial resolution allowed by this detector is too high if compared with the needing of the prototype (1 Mpix against about 100 pix requested). The prototype in its first version will acquire a redundant image that will be undersampled after the acquisition (before the application of data estimation algorithms). The estimation algorithms will be fed using the undersampled data only, while the comparison of

reconstructed signal with the full resolution image will be adopted as validation test. Figs. 2, 3, and 4 shows some views of the prototype.

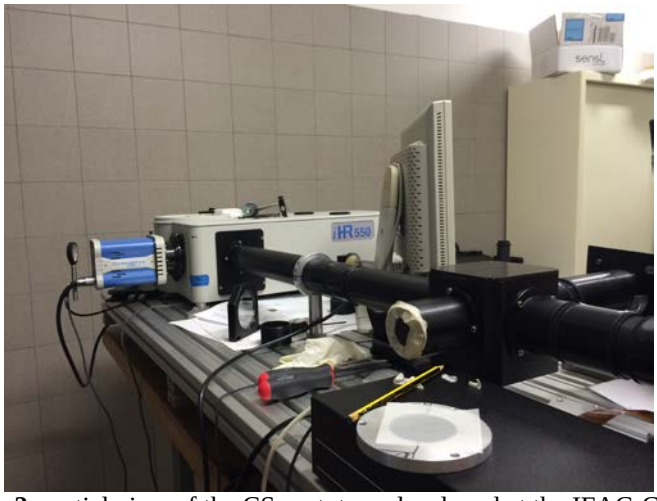


**Fig. 2.** partial view of the CS prototype developed at the IFAC-CNR.

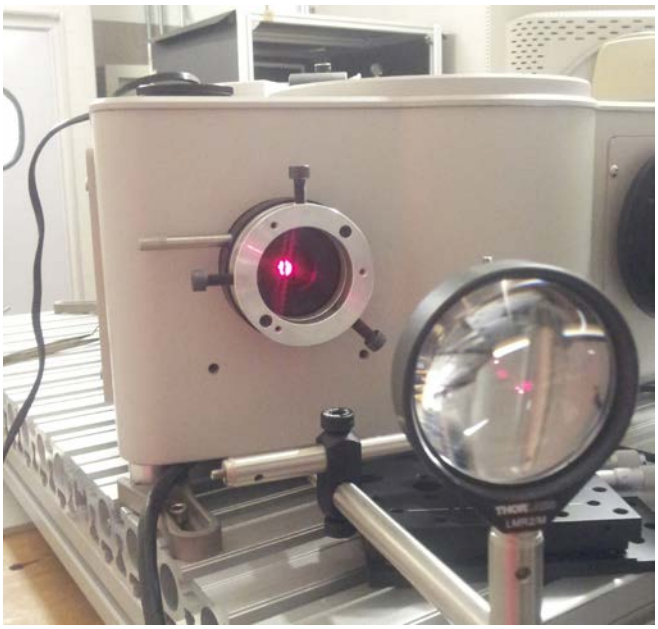

**Fig. 3.** Input port of the Joben Yvon spectrometer employed for the CS prototype illuminated by the laser diode source emitting around 650 nm. The input slit of the spectrometer is easily seen.

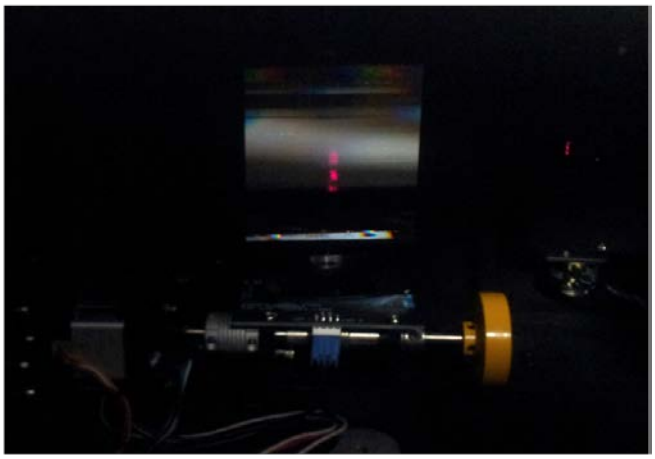

**Fig. 4.** Grating of the Joben Yvon spectrometer illuminated by the laser source of Fig. 3.

## III. PRELIMINARY EXPERIMENTAL RESULTS

Fig. 5 shows an example of spatial pattern displayed on the SLM. The same spatial pattern is seen by the instrument by the Dalsa camera as shown in Figs. 6, 7, 8, and 9. The light source for this acquisition is the red laser diode shown in Fig. 3.

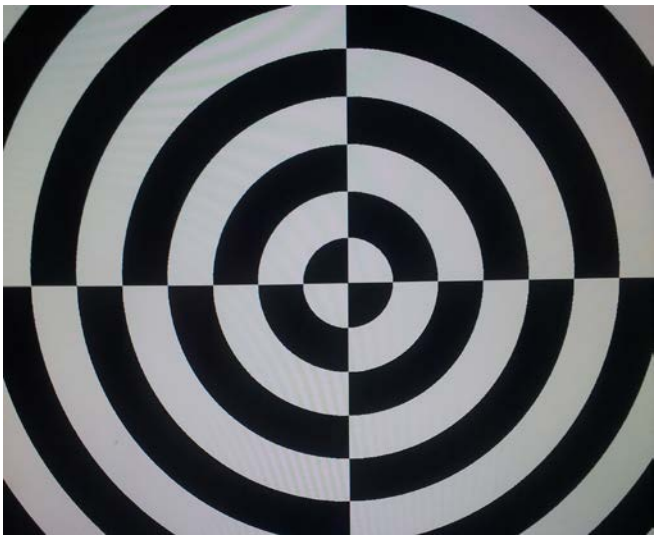

**Fig. 5.** Image impressed onto the liquid crystal SLM adopted for the development of the prototype.

It is worth noting that the final image collected by the prototype's detector (the Dalsa camera) is the product of the spectral image outputted by the selected spectrometer and the modulating 2d signal impressed on the spatial light modulator (SLM). The limited visibility in Figs. 6-9 of the SLM pattern depends on the spectro-spatial properties of the of the analyzed source. The red laser diode adopted for this acquisition exhibits its own spatial light distribution that is visible in Fig. 4. It is constituted by a bright central circular region surrounded by two short segments on the vertical direction (selected by the input slit of the spectrometer). The brighter region in the prototype image of Figs. 6-9 is the projection of the central circular spot of the laser source, which is expanded in the horizontal direction depending on the spectral density of power typical of this source. In this case the laser has a bandwidth around 1 nm - 2 nm that is broaden due to the large aperture imposed to the spectrometer input slit (about 1 mm). These circumstances offer a clear explication for the illumination distribution of the image in Figs. 6-9. Let us note the presence of a minor misalignment between the spectrometer and the CS arm of the prototype.

From the previous reasoning it is easily understood that the developed CS arm produces the optical implementation of a 2d modulation operator, in which the bidimensional modulating signal is programmed by means of the SLM device. The modulated signal is the spectral image at the output port of an imaging spectrometer operating in the pushbroom configuration.

Let $\rho_\lambda(x)$ indicate the ground scan line at the input port of the pushbroom spectrometer, $x$ being the spatial coordinate along the spectrometer's input slit and $\lambda$ the electromagnetic wavelength. The input signal $\rho_\lambda(x)$ has an implicit dependence on the spectral wavelength, meaning that for a given point source $x$ the EM power contributions related to different wavelengths $\lambda$ coincide in the same physical point. The spectral dispersion introduced by the spectrometer expands the spectral domain of the input signal, originating on its output port a 2d copy $\rho(x,\lambda)$ of $\rho_\lambda(x)$. The 2d image $m(\xi,\eta)$ displayed by the SLM directly modulates the signal $\rho(x,\lambda)$, as shown by the equation below.

$$\begin{aligned} s(\xi,\eta) &= \rho(x,\lambda)m(\xi,\eta) \\ (\xi,\eta) &= (x,\lambda)\mathbf{A} + (\xi_0,\eta_0) \end{aligned} \tag{1}$$

In this equation $\mathbf{A}$ is a coordinate transformation matrix relating the domains $(\xi,\eta)$ and $(x,\lambda)$, while the term $(\xi_0,\eta_0)$ is a simple origin shift.

**Fig. 6.** Image impressed onto the liquid crystal SLM as "seen" by the Dalsa camera of the prototype. The central wavelength of the measurement selected on the control SW of the spectrometer was 547.5 nm.

The origin shift is controlled by the optical configuration of the instrument as well as by the rotation of the spectrometer grating, i.e. the selected central wavelength for the current measurement. In a different wording the term $(\xi_0, \eta_0)$ changes when changing a different nominal wavelength for the spectrometer. An example of this behavior is shown by the pictures, from Fig. 6 up to Fig. 9. These figures show that the SLM pattern remains fixed within the field of view of the Dalsa camera, while a change of the nominal central wavelength of the spectrometer moves the output spot of the imaged source along the frame. In this way different sectors of the SLM patterns appear lighted at different nominal wavelengths. The wavelength axis increases from right toward left in the shown images, and a full frame covers a spectral interval around 12 nm.

**Fig. 7.** Image impressed onto the liquid crystal SLM as "seen" by the Dalsa camera of the prototype. The central wavelength of the measurement selected on the control SW of the spectrometer was 549.5 nm.

## IV. CONCLUSIONS

The next phase of the Project will aim at developing an experimental procedure for calibrating the geometric and radiometric parameters of the prototype. The calibration procedure fed with specific calibration measurements will be able to determine the parameters embedded in the coordinate transformation included in

(1). Moreover, the calibration will allow us to measure the radiometric response of the instrument to different reflectance levels impressed onto the SLM device.

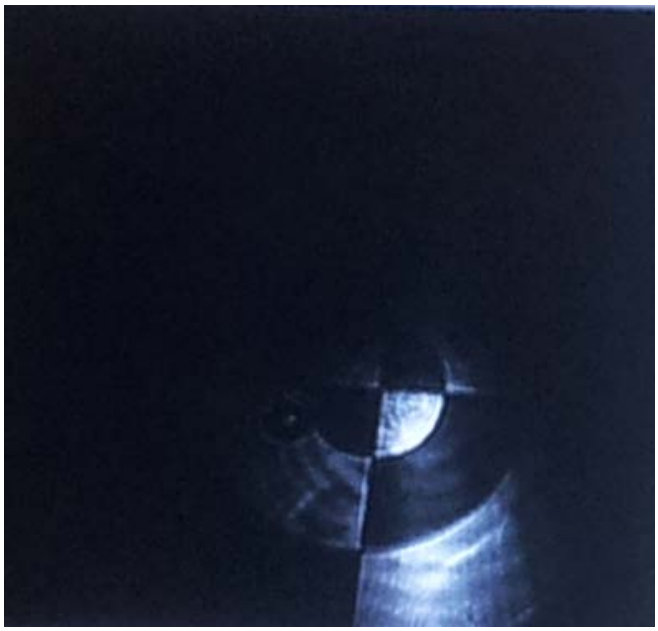

**Fig. 8.** Image impressed onto the liquid crystal SLM as "seen" by the Dalsa camera of the prototype. The central wavelength of the measurement selected on the control SW of the spectrometer was 551.5 nm.

**Fig. 9.** Image impressed onto the liquid crystal SLM as "seen" by the Dalsa camera of the prototype. The central wavelength of the measurement selected on the control SW of the spectrometer was 553.5 nm.

REFERENCES

[1] E. J. Candès, "Compressive sampling," Proceedings of the International Congress of Mathematicians, Madrid, Spain, European Mathematical Society (2006).
[2] E. J. Candès, J. Romberg, T. Tao, "Robust uncertainty principles: exact signal reconstruction from highly incomplete frequency information," *IEEE Trans. Inform. Theory*, vol. 52, pp. 489–509, 2006.
[3] E. Magli, M. Barni, A. Abrardo, A. Barducci, D. Guzzi, I. Pippi, "Technological issues in compressive sampling," Proc. International Workshop on On-Board Payload Data Compression (OBPDC), Barcelona, Spain, Oct. 29–30, 2012.
[4] A. Wagadarikar, R. John, R. Willet, and D. Brady, "Single disperser design for coded aperture snapshot spectral imaging," *Applied Optics*, 47, No. 10, pp.: B44-B51, 2008.

[5] M. E. Gehm, R. John, D. J. Brady, R. M. Willet, T. J. Schulz, "Single-shot compressive spectral imaging with a dual-disperser architecture," *Optics Express*, vol. 15, No. 21, pp. 14013-14027, 2007.
[6] R. J. Vaughan, N. L. Scott, and D. R. White, "The theory of bandpass sampling," *IEEE Trans. Signal Process.*, vol. 39, No. 9, pp. 1973–1984, 1991.
[7] A. Barducci, D. Guzzi, C. Lastri, P. Marcoionni, V. Nardino, I. Pippi, "Compressive Sensing and Hyperspectral Imaging," Proceedings of the 9th International Conference on Space Optics (ICSO 2012), Topics 2 Spectrometers - Hyperspectral instruments, in press (2012).
[8] P. B. Fellgett, "The multiplex advantage," Ph.D dissertation, University of Cambridge, Cambridge, UK, 1951.
[9] M. J. E. Golay, "Multislit spectrometry", Journal of Optical Society of America, vol. 39, pp. 437–444, 1949.
[10] E. E. Fenimore, and T. M. Cannon, "Coded Aperture Imaging with Uniformly Redundant Arrays," *Applied Optics*, vol. 17, No. 3, 1978.
[11] A. Barducci, D. Guzzi, C. Lastri, P. Marcoionni, V. Nardino, and I. Pippi (2010), "Radiometric and SNR properties of multiplex dispersive spectrometry", *Applied Optics*, vol. 49, No. 28, pp. 11622-11649, 2010.
[12] A. Barducci, "Information-theoretic approach to Fourier transform spectrometry", *Journal of the Optical Society of America B*, vol. 28, No. 4, pp. 637-648, 2011.
[13] A. Barducci, D. Guzzi, C. Lastri, P. Marcoionni, V. Nardino, I. Pippi, "Theoretical aspects of Fourier Transform Spectrometry and common path triangular interferometers," *Optics Express*, vol. 18, No. 11, pp. 11622–11649, 2010.
[14] S. K. Kuiteing, G. Coluccia, A. Barducci, M. Barni, E. Magli, " Compressive Hyperspectral Imaging Using Progressive Total Variation," Proceedings of the ICASSP 2014 Conference, Firenze (Italy), May 4-9, 2014.
[15] B. Aiazzi, L. Alparone, A. Barducci, S. Baronti, I. Pippi, "Information-Theoretic Assessment of Sampled Hyperspectral Imagers," *IEEE Transactions on Geoscience and Remote Sensing* , vol. 39, No. 7, pp. 1447–1458, 2001.